Insight into the $g \approx 16$ EPR Signals of Reduced Diiron–Oxo Proteins. Structure and Properties of $[Fe^{II}_2BPMP\{O_2P(OC_6H_5)_2\}_2]Cl$

Ho G. Jang, Michael P. Hendrich,* and Lawrence Que, Jr.*

Department of Chemistry, University of Minnesota, Minneapolis, Minnesota 55455

Received November 4, 1992

The diiron complexes $[Fe^{II}_2BPMP\{O_2P(OC_6H_5)_2\}_2]X$ (**1** (X = Cl), **2** (X = BF_4), **3** (X = BPh_4)) and $[Fe^{II}_2BPCP(O_2CC_2H_5)_2]BPh_4$ (**4**), where BPMP is the anion of 2,6-bis[(bis(2-pyridylmethyl)amino)methyl]-4-methylphenol and BPCP is the anion of 2,6-bis[(bis(2-pyridylmethyl)amino)methyl]-4-chlorophenol, have been synthesized to provide insight into the integer-spin EPR signals found in the diferrous forms of diiron–oxo proteins. Complex **1** crystallizes in the triclinic space group $P\bar{1}$ with cell constants a = 10.464(8) Å, b = 15.226(7) Å, c = 20.050(10) Å, α = 85.60(4)°, β = 88.38(5)°, γ = 74.98(5)°, V = 3076 Å^3 and Z = 2, with R = 0.049 and R_w = 0.069. It has a (μ-phenoxo)bis(μ-phosphato)diiron core, which affords an Fe–μ-O–Fe angle of 122.7(2)° and an Fe–Fe distance of 3.683(4) Å, values that are significantly larger than those for the corresponding propionate-bridged complex. Complex **4**, like $[Fe^{II}_2BPMP(O_2CC_2H_5)_2]BPh_4$ (**5**), exhibits a low field EPR signal near g = 17, similar to that found for deoxyhemerythrin azide. This resonance originates from a ground electronic state with integer spin, indicating that the metal centers are ferromagnetically coupled. Complexes **1–3** differ in two respects. They show EPR signals at g = 15, a resonance position that is incompatible with both strong and weak coupling models earlier proposed to explain the corresponding signals in **5**. However, the higher field position can be simulated by a rotation between the easy axes of magnetization of the iron sites in the weak coupling scheme. Secondly, the EPR signals of **1–3** arise from an excited state; thus the coupling interaction between the iron centers is found to be antiferromagnetic. The temperature dependence of the EPR signal indicates that the excited state is 12 cm^{-1} above the EPR silent ground state. These observations are corroborated by magnetization data for polycrystalline **2**. J is found to be 2.5–3.0 cm^{-1} ($\mathcal{H} = JS_1 \cdot S_2$) from fits of the multifield saturation magnetization data and the EPR temperature dependence with the constraint that the zero field splitting tensors of the individual ferrous ions are rotated 60° relative to each other along the easy axis of magnetization. The switch in sign of the iron–iron coupling interaction on going from the propionate-bridged complexes to the phosphate-bridged complexes undoubtedly results from the larger Fe–μ-O–Fe angle found in the latter complexes. The EPR properties observed for these complexes serve to validate the theoretical framework proposed by Hendrich et al. (*J. Am. Chem. Soc.* **1991**, *113*, 3039–3044) to rationalize the integer-spin EPR signals observed for the diferrous forms of diiron–oxo proteins and provide a foundation upon which to interpret the g = 15 signal recently observed for the diferrous R2 protein of ribonucleotide reductase.

Dinuclear iron–oxo centers[1] are the common structural component in the active sites of several metalloproteins such as hemerythrin (Hr),[2] the R2 protein of ribonucleotide reductase (RNR),[3] methane monooxygenase (MMO),[4] and the purple acid phosphatases (PAP).[5] The best characterized members of this class of proteins are Hr and RNR, which have (μ-oxo)diferric centers supported by carboxylate bridges in their oxidized forms.[6,7] Such structures have been reproduced in synthetic Fe(III)Fe(III) complexes by spontaneous self assembly methods; diiron complexes of this type have served as excellent models for the structural and spectroscopic properties of the diferric active sites.[1]

More recent interest has shifted to the diferrous active sites; such centers can be found in reduced forms of Hr,[8-10] MMO,[11] and RNR[12,13] and have been shown or postulated to be involved in dioxygen binding and/or activation chemistry. DeoxyHr has a (μ-hydroxo)bis(μ-carboxylato)diiron(II,II) core,[1,8,9] which is antiferromagnetically coupled and thus EPR silent with J estimated to be 20–30 cm^{-1} ($\mathcal{H} \approx JS_1 \cdot S_2$).[2,9,14] Addition of azide to deoxyHr elicits a low field EPR signal at g = 17;[9,10] the enhancement of the signal in parallel mode ($B_1 \parallel B$) indicates that

(1) (a) Que, L., Jr.; True, A. E. *Prog. Inorg. Chem.* **1990**, *38*, 98–200. (b) Sanders-Loehr, J. In *Iron Carriers and Iron Proteins*; Loehr, T. M., Ed.; VCH Publishers: New York, 1989; pp 373–466. (c) Que, L., Jr.; Scarrow, R. C. *ACS Symp. Ser.* **1988**, *372*, 159–178. (d) Lippard, S. J. *Angew. Chem., Int. Ed. Engl.* **1988**, *27*, 344–361.
(2) Wilkins, P. C.; Wilkins, R. G. *Coord. Chem. Rev.* **1987**, *79*, 195–214.
(3) Reichard, P.; Ehrenberg, A. *Science (Washington, D.C.)* **1983**, *221*, 514–519.
(4) (a) Fox, B. G.; Froland, W. A.; Dege, J. E.; Lipscomb, J. D. *J. Biol. Chem.* **1989**, *264*, 10023–10033. (b) Woodland, M. P.; Patil, D. S.; Cammack, R.; Dalton, H. *Biochim. Biophys. Acta* **1986**, *873*, 237–242. (c) Ericson, A.; Hedman, B.; Hodgson, K. O.; Green, J.; Dalton, H.; Bentsen, J. G.; Beer, R. H.; Lippard, S. J. *J. Am. Chem. Soc.* **1988**, *110*, 2330–2332. (d) DeWitt, J. G.; Bensten, J. G.; Rosenzweig, A. C.; Hedman, B.; Green, J.; Pilkington, S.; Papaefthymiou, G. C.; Dalton, H.; Hodgson, K. O.; Lippard, S. J. *J. Am. Chem. Soc.* **1991**, *113*, 9219–9235.
(5) (a) Antanaitis, B. C.; Aisen, P. *Adv. Inorg. Biochem.* **1983**, *5*, 111–136. (b) Averill, B. A.; Davis, J. C.; Burman, S.; Zirino, T.; Sanders-Loehr, J.; Loehr, T. M.; Sage, J. T.; Debrunner, P. G. *J. Am. Chem. Soc.* **1987**, *109*, 3760–3767.
(6) (a) Stenkamp, R. E.; Sieker, L. C.; Jensen, L. H. *J. Am. Chem. Soc.* **1984**, *106*, 618–622. (b) Sheriff, S.; Hendrickson, W. A.; Smith, J. L. *J. Mol. Biol.* **1987**, *197*, 273–296.
(7) Nordlund, P.; Sjöberg, B.-M.; Eklund, H. *Nature* **1990**, *345*, 593–598.
(8) (a) Holmes, M. A.; Trong, I. L.; Turley, S.; Sieker, L. C.; Stenkamp, R. E. *J. Mol. Biol.* **1991**, *218*, 583–593. (b) Stenkamp, R. E.; Sieker, L. C.; Jensen, L. H.; McCallum, J. D.; Sanders-Loehr, J. *Proc. Natl. Acad. Sci. U.S.A.* **1985**, *82*, 713–716. (c) Zhang, K.; Stern, E. A.; Ellis, F.; Sanders-Loehr, J.; Shiemke, A. K. *Biochemistry* **1988**, *27*, 7470–7479.
(9) (a) Reem, R. C.; Solomon, E. I. *J. Am. Chem. Soc.* **1984**, *106*, 8323–8325. (b) Reem, R. C.; Solomon, E. I. *J. Am. Chem. Soc.* **1987**, *109*, 1216–1226.
(10) Hendrich, M. P.; Pearce, L. L.; Que, L., Jr.; Chasteen, N. D.; Day, E. P. *J. Am. Chem. Soc.* **1991**, *113*, 3039–3044.
(11) (a) Fox, B. G.; Surerus, K. K.; Münck, E.; Lipscomb, J. D. *J. Biol. Chem.* **1988**, *263*, 10553–10556. (b) Hendrich, M. P.; Münck, E.; Fox, B. G.; Lipscomb, J. D. *J. Am. Chem. Soc.* **1990**, *112*, 5861–5865.
(12) Lynch, J. B.; Juarez-Garcia, C.; Münck, E.; Que, L., Jr. *J. Biol. Chem.* **1989**, *264*, 8091–8096.
(13) Sahlin, M.; Graslünd, A.; Petersson, L.; Ehrenberg, A.; Sjöberg, B.-M. *Biochemistry* **1989**, *28*, 2618–2625.
(14) Maroney, M. J.; Kurtz, D. M., Jr.; Nocek, J. M.; Pearce, L. L.; Que, L., Jr. *J. Am. Chem. Soc.* **1986**, 108, 6871.

0020-1669/93/1332-0911$04.00/0

it arises from a complex with integer spin. It has been suggested that this signal arises from a ferromagnetically coupled diferrous center resulting from the protonation of the hydroxo bridge.[9a] Similar low field EPR signals have been observed for the fully reduced form of the hydroxylase component of MMO at $g = 16$[11b] and for the diferrous form of the RNR R2 protein at $g \approx 15$.[15]

Hendrich et al.[10,11b,16] have developed a systematic approach to the analysis of integer spin EPR signals found for the diferrous states of the above proteins. The signals for deoxyHrN_3 and reduced MMO have been simulated and quantified within the framework of two electronic models that indicate ferromagnetic exchange coupling between the Fe(II) centers in the two complexes.[10,11b] However, the $g \approx 15$ signal of the RNR R2 protein is not understood because its higher field position relative to the signals found for deoxyHrN_3 and reduced MMO cannot be simulated with the simplifying assumptions used by the models that apply to the other proteins.

Synthetic diferrous complexes that mimic the EPR properties found for the above proteins are now available. $[Fe_2(OH)(Me_3TACN)_2(OAc)_2]ClO_4$[17] which reproduces the (μ-hydroxo)bis(μ-carboxylato)diiron(II,II) core found in deoxyHr is antiferromagnetically coupled ($J = 26\ cm^{-1}$) and EPR silent.[18] Similarly, $[Fe_2(N\text{-Et-HPTB})(OBz)](BF_4)_2$ which has a (μ-alkoxo)(μ-carboxylato)diiron(II,II) core is also antiferromagnetically coupled ($J = 22\ cm^{-1}$) and EPR silent.[19] Complexes that exhibit integer spin EPR signals include $[Fe^{II}_2BPMP(O_2CC_2H_5)_2]BPh_4$, which has a ($\mu$-phenoxo)bis($\mu$-carboxylato)diiron core and exhibits a signal at $g = 17$;[16] $[Fe^{II}_2(BIPhMe)_2(HCO_2)_4]$, which has a ($\mu$-formato-*O*)bis($\mu$-formato-*O*,*O*')diiron core and shows a signal at $g \approx 16$;[20] and $[Fe^{II}_2(Salmp)_2]^{2-}$ and $[Fe^{II}_2(H_2Hbab)_2(N\text{-MeIm})_2]$, which have ferromagnetically coupled bis(μ-phenoxo)diiron cores and exhibit signals at $g = 16$ and 12, respectively.[21] Of these latter complexes, only for $[Fe^{II}_2BPMP(O_2CC_2H_5)_2]BPh_4$ has a detailed parallel mode EPR study with spectral simulation been reported.[16]

In this paper, we report the structure and properties of a synthetic diferrous complex that exhibits an EPR signal at $g \approx 15$. This complex allows us to test the electronic models developed by Hendrich et al. and to extend the analysis to antiferromagnetically coupled systems. The high field position of the EPR signal observed for this complex in combination with spectral simulations allows us to differentiate between the two electronic models proposed. These studies lay a foundation upon which to base interpretations of integer-spin EPR signals derived from these fascinating diiron proteins.

Experimental Section

All reagents and solvents were purchased from commercial sources and used as received, unless noted otherwise. CH_2Cl_2 and CH_3CN were distilled under nitrogen from CaH_2 before use. 2,6-bis[(bis(2-pyridylmethyl)amino)methyl]-4-methylphenol (HBPMP) was synthesized according to published procedures.[16,22] The synthesis of 2,6-bis[(bis(2-pyridylmethyl)amino)methyl]-4-chlorophenol (HBPCP) followed the HBPMP method with 4-chlorophenol in place of 4-methylphenol: mp 108–109 °C; ^{1}H NMR ($CDCl_3$, 200 MHz) δ 3.76 (s, 4H), 3.85 (s, 8H), 7.15 (m, 4H), 7.24 (s, 2H), 7.50 (d, 4H), 7.65 (m, 4H), 8.50 (d, 4H). Microanalyses were performed by M-H-W Laboratories, Phoenix, AZ.

Bis(μ-diphenyl phosphato-*O*,*O*')[2,6-bis[(bis(2-pyridylmethyl)amino)methyl]-4-methylphenolato]diiron(II,II) Chloride, $[Fe^{II}_2BPMP\{O_2P(OC_6H_5)_2\}_2]Cl$ (1). A solution of 0.200 g (0.377 mmol) HBPMP in 15 mL methanol was treated under argon with a solution of 0.123 g (0.754 mmol) $FeCl_2{\cdot}2H_2O$ in 10 mL methanol. The resulting greenish yellow solution was treated with a 5 mL methanol solution of 0.236 g (0.943 mmol) phosphoric acid, diphenyl ester and 0.13 mL (0.943 mmol) triethylamine, thereby resulting in the precipitation of a crude yellow product. Further purification was achieved by recrystallization of the crude product by vapor diffusion of acetone into a dichloromethane solution of **1** to afford yellow-orange crystals. Diffraction quality crystals were obtained by layering acetone over a dichloromethane solution of **1**; these crystals contained two molecules of occluded dichloromethane and one of water. However, these dichloromethane solvate molecules were absent in the vacuum-dried microanalysis sample. Anal. Calcd for $C_{57}H_{55}ClFe_2N_6O_{10}P_2$: C, 57.38; H, 4.65; N, 7.04; P, 5.19. Found: C, 57.30; H, 4.91; N, 7.05; P, 5.34.

Bis(μ-diphenyl phosphato-*O*,*O*')[2,6-bis[(bis(2-pyridylmethyl)amino)methyl]-4-methylphenolato]diiron(II,II) Tetrafluoroborate, $[Fe^{II}_2BPMP\{O_2P(OC_6H_5)_2\}_2]BF_4$ (2). This complex was prepared using the same experimental procedure outlined for **1**, with $Fe(BF_4)_2{\cdot}6H_2O$ in place of $FeCl_2{\cdot}2H_2O$. After recrystallization of the crude product by vapor diffusion of acetone into a dichloromethane solution of **2**, yellow orange microcrystals were obtained by diffusion of ether into an acetonitrile solution of **2**. Anal. Calcd for $C_{57}H_{53}BF_4Fe_2N_6O_9P_2$: C, 55.82; H, 4.36; N, 6.85; P, 5.05. Found: C, 55.70; H, 4.37; N, 6.90; P, 5.29.

Bis(μ-diphenyl phosphato-*O*,*O*')[2,6-bis[(bis(2-pyridylmethyl)amino)methyl]-4-methylphenolato]diiron(II,II) Tetraphenylborate, $[Fe^{II}_2BPMP\{O_2P(OC_6H_5)_2\}_2]BPh_4$ (3). A solution of 0.200 g (0.377 mmol) HBPMP in 10 mL acetonitrile was treated under argon with a solution of 0.254 g (0.754 mmol) $Fe(BF_4)_2{\cdot}6H_2O$ in 10 mL acetonitrile. The resulting yellow solution was treated with a 5 mL acetonitrile solution of of 0.236 g (0.943 mmol) phosphoric acid, diphenyl ester and 0.13 mL triethylamine. Metathesis with sodium tetraphenylborate (0.168 g, 0.490 mmol) and evaporation of solvent resulted in the precipitation of the crude product. Further purification was achieved by recrystallization of the crude product by vapor diffusion of ether into an acetonitrile solution of **3** to afford yellow-orange microcrystals of **3**. Anal. Calcd for $C_{81}H_{73}BFe_2N_6O_9P_2$: C, 66.68; H, 5.04; N, 5.76; P, 4.25. Found: C, 66.38; H, 5.13; N, 5.73; P, 4.39.

Bis(μ-propionato-*O*,*O*')[2,6-bis[(bis(2-pyridylmethyl)amino)methyl]-4-chlorophenolato]diiron(II,II) Tetraphenylborate, $[Fe^{II}_2BPCP(O_2CC_2H_5)_2]BPh_4$ (4). A solution of 0.250 g (0.454 mmol) HBPCP in 10 mL methanol was treated under argon with a solution of 0.306 g (0.908 mmol) $Fe(BF_4)_2{\cdot}6H_2O$ in 10 mL methanol. The resulting tan solution was treated with 0.13 g (1.36 mmol) sodium propionate in 5 mL methanol, thereby forming an orange-yellow solution. Metathesis with sodium tetraphenylborate (0.202 g, 0.590 mmol) resulted in the immediate precipitation of the crude product. Further purification was achieved by recrystallization of the crude product by vapor diffusion of acetone into a dichloromethane solution of **4** to afford orange microcrystals. These crystals contained one dichloromethane solvate molecule as determined from microanalysis. ^{1}H NMR (CD_2Cl_2, 300 MHz): δ BPMP-CH_2, 185, 79, 74, 73, –15, –30; py *o*-H, 176, 151; py *m*-H, 62, 42, 42, 28; py *p*-H, 13, 13; phenolate *m*-H, 26; propionate CH_2, 55, 42; propionate CH_3, 12. Anal. Calcd for $C_{63}H_{62}BCl_3Fe_2N_6O_5$: C, 62.43; H, 5.16; N, 6.93; Cl, 8.77. Found: C, 62.62; H, 5.36; N, 6.94; Cl, 8.63.

Crystallographic Results for $[Fe^{II}_2BPMP\{O_2P(OC_6H_5)_2\}_2]Cl{\cdot}2CH_2Cl_2{\cdot}H_2O$ (1). A yellow-orange crystal of $[Fe^{II}_2BPMP\{O_2P(OC_6H_5)_2\}_2]Cl{\cdot}2CH_2Cl_2{\cdot}H_2O$ (dimensions: 0.60 × 0.50 × 0.35 mm) was

(15) Hendrich, M. P.; Elgren, T. E.; Que, L., Jr. Unpublished observations.
(16) Borovik, A. S.; Hendrich, M. P.; Holman, T. R.; Münck, E.; Papaefthymiou, V.; Que, L., Jr. *J. Am. Chem. Soc.* **1990**, *112*, 6031–6038.
(17) Abbreviations used: Me_3TACN, 1,4,7-trimethyl-1,4,7-triazacyclononane; *N*-Et-HPTB, *N*,*N*,*N*',*N*'-tetrakis(*N*-ethyl-2-benzimidazolylmethyl)-2-hydroxy-1,3-diaminopropane; OBz, benzoate anion; HBPMP, 2,6-bis[(bis(2-pyridylmethyl)amino)methyl]-4-methylphenol; BIPhMe, bis(2-(1-methylimidazolyl)phenyl)methoxymethane; H_4Hbab, 1,2-bis(hydroxybenzamido)benzene; Hsalmp, bis(salicylideneamino)-2-methylphenol; $HB(pz)_3$, hydrotris(1-pyrazolyl)borate; TPA, tris(2-pyridylmethyl)amine.
(18) (a) Chaudhuri, P.; Wieghardt, K.; Nuber, B.; Weiss, J. *Angew. Chem., Int. Ed. Engl.* **1985**, *24*, 778–779. (b) Hartman, J. R.; Rardin, R. L.; Chaudhuri, P.; Pohl, K.; Wieghardt, K.; Nuber, B.; Weiss, J.; Papaefthymiou, G. C.; Frankel, R. B.; Lippard, S. J. *J. Am. Chem. Soc.* **1987**, 109, 7387–7396.
(19) Ménage, S.; Brennan, B. A.; Juarez-Garcia, C.; Münck, E.; Que, L., Jr. *J. Am. Chem. Soc.* **1990**, *112*, 6423–6425.
(20) (a) Tolman, W. B.; Bino, A.; Lippard, S. J. *J. Am. Chem. Soc.* **1989**, *111*, 8522–8523. (b) Tolman, W. B.; Liu, S.; Bentsen, J. G.; Lippard, S. J. *J. Am. Chem. Soc.* **1991**, *113*, 152–164.
(21) (a) Snyder, B. S.; Patterson, G. S.; Abrahamson, A. J.; Holm, R. H. *J. Am. Chem. Soc.* **1989**, *111*, 5214–5223. (b) Stassinopoulos, A.; Schulte, G.; Papaefthymiou, G. C.; Caradonna, J. P. *J. Am. Chem. Soc.* **1991**, *113*, 8686–8697.
(22) (a) Suzuki, M.; Kanatomi, H.; Murase, I. *Chem. Lett., Chem. Soc. Jpn.* **1981**, 1745–1748. (b) Suzuki, M.; Uehara, A.; Oshio, H.; Endo, K.; Yanaga, M.; Kida, S.; Satito, K. *Bull. Chem. Soc. Jpn.* **1987**, *60*, 3547–3555.

Table I. Crystallographic Experimental Data and Computations[a] for **1**

formula	$C_{59}H_{59}N_6Cl_5Fe_2O_{10}P_2$	ρ(calc), g cm^{-3}	1.469
		radiation (λ, Å)	Mo Kα (0.7107)
fw	1363.05	$\mu_{Mo\ K\alpha}$, cm^{-1}	8.01
T, K	172	scan type	ω
cryst syst	triclinic	$2\theta_{max}$, deg	49.9
space group	$P\bar{1}$ (No. 2)	no. of reflns	10 796
a, Å	10.464(8)	no. of unique data	6974
b, Å	15.226(7)	with $I > 3\sigma(I)$	
c, Å	20.050(10)	no. of variables	757
α, deg	85.60(4)	R^b	0.049
β, deg	88.38(5)	$R_w{}^b$	0.069
γ, deg	74.98(5)		
V, Å^3	3076(6)		
Z	2		

[a] The intensity data were processed as described in: *CAD 4 and SDP-PLUS User's Manual*; B. A. Frenz & Associates: College Station, TX, 1982. The net intensity $I = [K(NPI)](C - 2B)$, where $K = 20.1166$ (attenuator factor), NPI = ratio of fastest possible scan rate to scan rate for the measurement, C = total count, and B = total background count. The standard deviation in the net intensity is given by $[\sigma(I)]^2 = (K/NPI)^2[C + 4B + (pI)^2]$, where p is a factor used to downweight intense reflections. The observed structure factor amplitude F_o is given by $F_o = (I/Lp)^{1/2}$, where Lp = Lorentz–polarization factor. The $\sigma(I)$'s were converted to the estimated errors in the relative structure factors $\sigma(F_o)$ by $\sigma(F_o) = {}^1/_2[\sigma(I)/I]F_o$. [b] $R = (\sum||F_o| - |F_c||)/(\sum F_o)$; $R_w = [(\sum w|F_o - F_c|^2)/(\sum w(F_o)^2)]^{1/2}$.

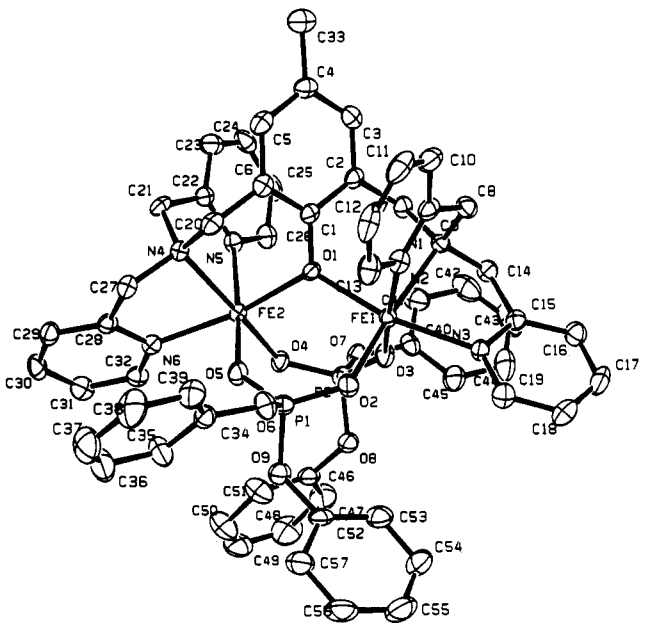

Figure 1. ORTEP plot of the structure of **1**, $[Fe_2BPMP\{O_2P(OC_6H_5)_2\}_2]^+$, showing 50% probability ellipsoids. The hydrogen atoms are omitted for clarity.

mounted on the end of a glass fiber with a viscous high-molecular-weight hydrocarbon. Intensity data were collected at the Crystallography Facility of the University of Minnesota Chemistry Department on an Enraf-Nonius CAD4 diffractometer. Absorption corrections were applied for Lorentz and polarization effects, but it was unnecessary to correct for crystal decay and absorption. The cell dimensions were obtained by least-squares refinements of the setting angles for 25 carefully centered reflections ($2\theta = 22.2 - 36.8°$). The structure was solved by using direct methods and standard difference Fourier routines in the TEXSAN crystallographic software package of the Molecular Structure Corp. The crystallographic and refinement data are summarized in Table I. All non-H atoms were refined with anisotropic thermal parameters. Hydrogen atoms were included in the structure factor correlation in idealized positions (d(C–H) = 0.95 Å, $B_H = 3.0$ Å^2). The standard deviation of an observation of unit weight was 1.77. The weighting scheme was based on counting statistics and included a factor ($p = 0.05$) to downweight the intense reflections. The maximum and minimum peaks on the final difference Fourier map corresponded to 1.56 and –0.43 e/Å^3, respectively. Neutral atom scattering factors (including anomalous scattering) were used.[23]

Table II. Selected Bond Lengths (Å) and Angles (deg) for **1**[a]

a. Bond Lengths

Fe1–O1	2.086(4)	Fe2–O1	2.110(4)
Fe1–O2	2.023(4)	Fe2–O4	2.043(4)
Fe1–O3	2.138(4)	Fe2–O5	2.132(4)
Fe1–N1	2.209(5)	Fe2–N4	2.208(5)
Fe1–N2	2.174(5)	Fe2–N5	2.169(5)
Fe1–N3	2.184(5)	Fe2–N6	2.171(5)
P1–O2	1.491(4)	P2–O3	1.483(4)
P1–O5	1.468(4)	P2–O4	1.495(4)
P1–O6	1.597(4)	P2–O7	1.609(4)
P1–O9	1.604(4)	P2–O8	1.597(4)
O1–C1	1.326(6)	O6–C34	1.395(7)
O7–C40	1.398(7)	O8–C46	1.398(7)
O9–C52	1.391(7)	N1–C7	1.493(7)
N1–C8	1.488(7)	N1–C14	1.472(7)
N2–C9	1.336(7)	N2–C13	1.343(7)
N3–C15	1.344(7)	N3–C19	1.326(7)
N4–C20	1.500(7)	N4–C21	1.478(7)
N4–C27	1.484(7)	N5–C22	1.349(7)
N5–C26	1.353(7)	N6–C28	1.353(7)
N6–C32	1.350(7)	C1–C2	1.403(8)
C1–C6	1.401(8)	C2–C3	1.394(8)
C2–C7	1.507(8)	C3–C4	1.394(8)
C4–C5	1.385(8)	C4–C33	1.512(8)
C5–C6	1.397(8)	C6–C20	1.508(8)
C8–C9	1.514(8)	C9–C10	1.395(8)
C10–C11	1.381(9)	C11–C12	1.360(9)
C12–C13	1.384(9)	C14–C15	1.504(8)
C15–C16	1.387(8)	C16–C17	1.383(9)
C17–C18	1.360(9)	C18–C19	1.396(8)
C21–C22	1.501(8)	C22–C23	1.381(8)
C23–C24	1.383(9)	C24–C25	1.371(9)
C25–C26	1.370(9)	C27–C28	1.507(8)
C28–C29	1.375(8)	C29–C30	1.388(8)
C30–C31	1.385(9)	C31–C32	1.377(8)
	Fe1–Fe2	3.683(4)	

b. Bond Angles (deg)

O1–Fe1–O2	98.0(2)	O1–Fe2–O4	99.1(2)
O1–Fe1–O3	87.6(2)	O1–Fe2–O5	88.0(1)
O1–Fe1–N1	88.7(2)	O1–Fe2–N4	88.5(2)
O1–Fe1–N2	90.7(2)	O1–Fe2–N5	88.2(2)
O1–Fe1–N3	162.7(2)	O1–Fe2–N6	163.3(2)
O2–Fe1–O3	97.8(2)	O4–Fe2–O5	98.5(2)
O2–Fe1–N1	169.3(2)	O4–Fe2–N4	167.8(2)
O2–Fe1–N2	92.6(2)	O4–Fe2–N5	92.1(2)
O2–Fe1–N3	98.4(2)	O4–Fe2–N6	97.0(2)
O3–Fe1–N1	90.7(2)	O5–Fe2–N4	91.2(2)
O3–Fe1–N2	169.6(2)	O5–Fe2–N5	169.2(2)
O3–Fe1–N3	84.7(2)	O5–Fe2–N6	85.2(2)
N1–Fe1–N2	78.9(2)	N4–Fe2–N5	78.5(2)
N1–Fe1–N3	75.9(2)	N4–Fe2–N6	76.4(2)
N2–Fe1–N3	94.0(2)	N5–Fe2–N6	95.6(2)
Fe1–O1–C1	118.5(3)	Fe2–O1–C1	118.8(8)
Fe1–O2–P1	131.0(2)	Fe2–O4–P2	129.1(2)
Fe1–O3–P2	137.7(2)	Fe2–O5–P1	136.7(2)
O2–P1–O5	121.5(2)	O3–P2–O4	121.6(2)
O2–P1–O6	103.4(2)	O3–P2–O7	109.6(2)
O2–P1–O9	109.5(2)	O3–P2–O8	106.3(2)
O5–P1–O6	110.5(2)	O4–P2–O7	103.9(2)
O5–P1–O9	105.6(2)	O4–P2–O8	109.4(2)
O6–P1–O9	105.4(2)	O7–P2–O8	104.9(2)
P1–O6–C34	126.6(4)	P2–O7–C40	123.2(4)
P1–O9–C52	121.2(3)	P2–O8–C46	122.2(4)
Fe1–N1–C7	110.5(3)	Fe2–N4–C20	109.7(3)
Fe1–N1–C8	109.1(3)	Fe2–N4–C21	109.3(3)
Fe1–N1–C14	105.5(3)	Fe2–N4–C27	105.4(3)
Fe1–N2–C9	114.7(4)	Fe2–N5–C22	114.4(4)
Fe1–N2–C13	126.0(4)	Fe2–N5–C26	125.5(4)
Fe1–N3–C15	114.1(4)	Fe2–N6–C28	114.8(4)
Fe1–N3–C19	127.2(4)	Fe2–N6–C32	126.7(4)
	Fe1–O1–Fe2	122.7(2)	

[a] Estimated standard deviations in the least significant digits are given in parentheses.

An ORTEP plot of the structure of the cation is shown in Figure 1, together with the numbering scheme for the complex. Selected bond lengths and bond angles are listed in Table II, while atomic coordinates,

Table III. Comparison of the Properties of the Diiron(II) Complexes

property	1[a]	5[b]	6[c]	7[d]	8[e]	9[f]	10[g]
Fe–μ-OR, Å	2.086(4)	2.052(1)	1.987(8)	1.960(6)	2.113(2)	2.137(8)	1.997(7)
	2.110(4)	2.062(1)		1.973(7)	2.172(2)	2.182(8)	2.167(7)
Fe–μ-O_2X-*O,O'*, Å	2.033(4)	2.040(2)	2.120(10)	2.017(8)	2.067(3)	n.a.	n.a.
	2.135(4)	2.144(2)	2.142(9)	2.056(7)	2.156(2)		
Fe···Fe, Å	3.683(4)	3.348(1)	3.32(1)	3.473(4)	3.5936(8)	3.202(2)	3.165(7)
Fe–μ-O–Fe, deg	122.7(2)	108.93(6)	113.2(2)	124.0(3)	113.0(1)	95.6(3)	98.9(3)
						95.9(3)	
J, cm^{-1} ($\mathcal{H} = JS_1 \cdot S_2$)	2.5–3.0	<0[h]	26	21	~0.3	−2.4	−5.0
EPR	$g \approx 15$	$g \approx 17$	silent	silent	$g \approx 16$	$g \approx 16$[h]	$g \approx 12$

[a] $[Fe_2BPMP\{O_2P(OC_6H_5)_2\}_2]^+$. [b] $[Fe_2BPMP(O_2CC_2H_5)_2]^+$; ref 16. [c] $[Fe_2(OH)(OAc)_2(Me_3TACN)_2]^+$; ref 18. [d] $[Fe_2(N\text{-Et-HPTB})(OBz)]^{2+}$; ref 19. [e] $[Fe_2(BIPhMe)_2(O_2CH)_4]$; ref 20. [f] $[Fe_2(Salmp)_2]^{2-}$; ref 21a. [g] $[Fe_2(H_2Hbab)_2(N\text{-Me-Im})_2]$; ref 21b. [h] Unpublished results.

thermal parameters, and a complete listing of bond lengths and angles are available as supplementary material.

Physical Methods. All solution samples were prepared under argon. Visible spectra of the complexes were obtained using a Hewlett Packard 8451A diode array spectrophotometer. ^{1}H NMR spectra of the dinuclear metal complexes were obtained on IBM AC-300 and Varian VXR-300 NMR spectrometers. All spectra were obtained using a 90° pulse with 16K data points. An inversion-recovery pulse sequence (180°–τ–90°–Acq) was used to obtain nonselective proton longitudinal relaxation times (T_1) with the carrier frequency set at several different positions to ensure the validity of the measurements.

X-band EPR measurements were performed with a Varian E9 spectrometer equipped with an Oxford liquid helium cryostat. A Varian E-236 bimodal cavity was used to generate the microwave fields parallel and perpendicular to the static field. The microwave frequency was measured with a frequency counter, and the magnetic field was calibrated with an NMR gaussmeter to afford a field uncertainty of ±0.1 mT. For the temperature dependence study, a calibrated carbon glass resistor (CGR-1-1000, Lakeshore Cryotronics) was immersed in the sample and sealed with wax. The EPR tube was positioned vertically to minimize impurity signals from the resistor. The leads of the resistor were replaced with a phosphor bronze wire to minimize heat input. Samples were prepared under argon, with all solvents distilled prior to use and degassed by three freeze–pump–thaw cycles.

Multifield saturation magnetization data were collected as described previously[24] with a Quantum Design superconducting susceptometer from 2 to 300 K at fixed fields ranging from 1.0 to 5.0 T. Polycrystalline samples (typically 20 mg) were ground thoroughly to give a powder average magnetization in the applied field and held in place between gel cap halves which have no detectable paramagnetic impurities. The independence of the susceptibility verus the magnetic field was checked at room temperature. The magnetization data were corrected for diamagnetism using the Pascal's constant for the complex.[25] Theoretical powder average magnetization curves were calculated from the spin Hamiltonian shown in eq 1,[24] where J is the isotropic exchange coupling constant, D_i

$$\mathcal{H} = JS_1 \cdot S_2 + \sum [D_i({S_{zi}}^2 - 2) + E_i({S_{xi}}^2 - {S_{yi}}^2) + \beta \mathbf{S}_i \cdot \mathbf{g}_i \cdot \mathbf{B}]_{i=1,2} \quad (1)$$

and E_i are the axial and rhombic zero-field splitting parameters, and $\mathbf{g}_i$ are the $\mathbf{g}$ tensors of the uncoupled sites. The saturation magnetization difference data (sample minus control) were fit by the simplex method[26] to find the spin Hamiltonian parameters yielding the minimum in the standard quality of fit parameter, χ^2, where $\chi^2 = \Sigma(\text{Moment}_{exp} - \text{Moment}_{fit})^2$. The final fits did not require the inclusion of mononuclear paramagnetic impurities. Uncertainties in the spin Hamiltonian parameters reflect the results of fitting data collected from the two independently prepared samples. The amount of paramagnetism found from the fitting process was used to scale the vertical axes of the plots.

Results and Discussion

Several synthetic diferrous complexes have been reported to exhibit integer-spin EPR signals like those found for diferrous centers in Hr and MMO.[9-11] The previously reported model complex $[Fe^{II}_2BPMP(O_2CC_2H_5)_2]BPh_4$ (**5**) shows an EPR signal at $g = 17$ arising from a ferromagnetically coupled diferrous system.[16] This is thus far the only synthetic complex for which a detailed EPR analysis, including simulations, has been performed. On the other hand, $[Fe^{II}_2(BIPhMe)_2(O_2CH)_4]$ (**8**) shows EPR signals near $g \approx 16$ despite its being a diferrous system with weak antiferromagnetic coupling ($J = 0.32$ cm^{-1}), but the EPR properties of this complex are not well understood.[20] In order to further elucidate the role the metal-metal interaction plays in determining the spin physics of diferrous sites, we have synthesized variants of complex **5** and examined the effects that structural changes have on the EPR properties. First, the complex $[Fe^{II}_2BPCP(O_2CC_2H_5)_2]BPh_4$ (**4**) was synthesized, where the 4-methyl group on the phenol was replaced by Cl, in order to determine the effects of changing the basicity of the μ-phenoxo group. Second, the complexes $[Fe^{II}_2BPMP\{O_2P(OC_6H_5)_2\}_2]X$, where X is Cl, BF_4, and BPh_4, were prepared to incorporate a bridging anion with a larger bite and thus increase the Fe–μ-O–Fe angle. Only the Cl salt (**1**) afforded diffraction quality crystals, and its structure was determined.

Solid-State Structure of $[Fe^{II}_2BPMP\{O_2P(OC_6H_5)_2\}_2]Cl\cdot 2CH_2Cl_2\cdot H_2O$ (1). The structure of **1** (Figure 1) shows two iron centers bridged by the phenolate oxygen atom of $BPMP^-$ and by two diphenyl phosphate bridging ligands. This triply bridged core structure has been observed for $Fe^{III}Fe^{III}$,[27,28] $Fe^{III}Fe^{II}$,[29] and $Fe^{III}Zn^{II}$ [29] complexes, but **1** is the first $Fe^{II}Fe^{II}$ complex with such a core structure.

The core structure of **1** is compared in Table III with those of other structurally characterized diferrous complexes $[Fe_2BPMP(O_2CC_2H_5)_2]BPh_4$ (**5**),[16] $[Fe_2(OH)(OAc)_2(Me_3TACN)_2]ClO_4$ (**6**),[18] $[Fe_2(N\text{-Et-HPTB})(OBz)](BF_4)_2$ (**7**),[19] $[Fe_2(BIPhMe)_2(O_2CH)_4]$ (**8**),[20] $(Et_4N)_2[Fe_2(Salmp)_2]$ (**9**),[21a] and $[Fe_2(H_2Hbab)_2(N\text{-Me-Im})_2]$ (**10**).[21b] The Fe1–μ-O1 and Fe2–μ-O1 bond lengths of **1** are 2.086(4) and 2.110(4) Å, respectively; these values are intermediate between those of **6** and **7** on one hand and **8** on the other, consistent with the intermediate basicity of the phenolate relative to those of hydroxide, alkoxide, and formate. The Fe–μ-O bonds are slightly longer than those of **5**; similar differences are observed for the Fe–μ-O bond lengths of (μ-oxo)diferric complexes with acetate and diphenyl phosphate bridges.[28,30] Both the bridging phosphates in **1** are bound unsymmetrically to the diiron unit, with phosphate 1 more strongly bound to Fe1 and phosphate 2 more strongly bound to Fe2. This bridging arrangement is also observed for **5** and $[Fe_2(5\text{-Me-HXTA})(OAc)_2]^-$ [31] and can be attributed to the ligands

(23) *International Tables for X-ray Crystallography*; Kynoch Press: Birmingham, England, 1974; Vol. IV, Table 2.2 A.
(24) Day, E. P.; Kent, T. A.; Lindahl, P. A.; Münck, E.; Orme-Johnson, W. H.; Roder, H.; Roy, A. *Biophys. J.* **1987**, *52*, 837–853.
(25) Boudreaux, E. A.; Mulay, L. N. *Theory and Applications of Molecular Paramagnetism*; John Wiley and Sons: New York, 1976.
(26) Nelder, J.; Mead, R. *Comput. J.* **1965**, 308–313.
(27) Drüeke, S.; Wieghardt, K.; Nuber, B.; Weiss, J.; Fleischhhauer, H.; Gehring, S.; Haase, W. *J. Am. Chem. Soc.* **1989**, *111*, 8622–8631.
(28) Turowski, P. N.; Amstrong, W. H.; Roth, M. E.; Lippard, S. J. *J. Am. Chem. Soc.* **1990**, *112*, 681–690.
(29) Schepers, K.; Bremer, B.; Krebs, B.; Henkel, G.; Althaus, E.; Mosel, B.; Miller-Warmuth, W. *Angew. Chem., Int. Ed. Engl.* **1990**, *29*, 531–533.
(30) Norman, R. E.; Yan, S.; Que, L., Jr.; Backes, G.; Ling, J.; Sanders-Loehr, J.; Zhang, J. H.; O'Connor, C. J. *J. Am. Chem. Soc.* **1990**, *112*, 1554–1562.
(31) Murch, B. P.; Bradley, F. C.; Que, L., Jr. *J. Am. Chem. Soc.* **1986**, *108*, 5027–5028.

trans to the bridging anions. The shorter Fe–O(bridging anion) bond is invariably trans to the tertiary amine bond. The Fe–O(bridging anion) distances in **1** are comparable to those of the carboxylate-bridged **5**. The Fe–N bond lengths in **1** are unremarkable.

The Fe–Fe distance in **1** (3.683(4) Å) is significantly larger than that of **5** (3.348(2) Å) due to the larger bite of the bridging phosphate. The Fe–Fe distances of other phosphate-bridged complexes similarly increase when compared to those of their carboxylate-bridged analogues, e.g., 3.335(1) Å for $[Fe^{III}_2O\{O_2P(OC_6H_5)_2\}_2(HB(pz)_3)_2]$ versus 3.149(1) Å for $[Fe^{III}_2O(OAc)_2(HB(pz)_3)_2]$[28] and 3.357(3) Å for $[Fe^{III}_2O\{O_2P(OC_6H_5)_2\}(TPA)_2]^{3+}$ versus 3.243(1) Å for $[Fe^{III}_2O(OAc)(TPA)_2]^{3+}$.[30] However, the metal–metal distance in **1** is comparable to that in $[Fe^{III}Zn^{II}BPMP\{O_2P(OC_6H_5)_2\}_2]^{2+}$ (3.695(1) Å).[29] The Fe–μ-O–Fe angle of 122.7(2)° is the largest among the triply-bridged diiron(II) complexes. This larger Fe–μ-O–Fe angle is also found in other phosphate-bridged complexes: 123.2(3)° for $[(Me_3TACN)_2Fe^{III}_2O\{O_3P(OC_6H_5)\}_2]$,[27] 134.7(2)° for $[Fe^{III}_2O\{O_2P(OC_6H_5)_2\}_2(HB(pz)_3)_2]$,[28] and 122.8(1)° for $[Fe^{III}Zn^{II}BPMP\{O_2P(OC_6H_5)_2\}_2]^{2+}$.[29]

Complex **1** does not exhibit any crystallographically imposed symmetry, but there is a pseudo twofold axis about the C1–O1 bond. The BPMP ligand adopts a conformation that is similar to those observed in structures of other BPMP complexes.[16] The phenyl ring of the $BPMP^-$ ligand is twisted relative to the Fe1–O1–Fe2 plane, resulting in a dihedral angle of 54° between the plane defined by the C1–C6 carbon atoms of the phenolate ring and the Fe1–O1–Fe2 plane. This twist of the phenolate ring relative to the Fe1–O1–Fe2 plane is also observed in **5** with a dihedral angle of 48°.[16]

Electronic Absorption and NMR Properties. Complex **5** has been reported to exhibit a visible absorption band centered at 422 nm ($\epsilon \approx 2.3$ mM^{-1} cm^{-1}) in CH_2Cl_2.[16] This band shifts to 442 nm ($\epsilon \approx 3.0$ mM^{-1} cm^{-1}) upon substitution of BPMP with the more electron withdrawing BPCP in **4** and to 432 nm ($\epsilon \approx 2.9$ mM^{-1} cm^{-1}) upon substitution of the propionate bridges in **5** with diphenyl phosphate bridges in **1–3**.

The ^1H NMR spectra of complexes **1–5** exhibit well-resolved sharp resonances that have a chemical shift range which spans over 240 ppm (Figure 2). The relatively sharp isotropically shifted resonances are a result of the fast electronic relaxation rates of these high spin Fe(II) centers.[32] The assignment of these features for **2** has been accomplished using T_1 and COSY data and is reported elsewhere.[33] The spectral patterns of **4** and **5**, not surprisingly, are quite similar except for the absence of the phenolate p-CH_3 peak in **4** (see Figure 2). Interestingly, the peaks for the propionate CH_2 protons are found at 42 and 55 ppm for **4** and 37 and 50 ppm for **5**, reflecting the stronger interaction of the propionate with the diiron center in **4** in response to the decrease in the phenolate basicity. The spectral pattern for **1** differs from those of **4** and **5**, particularly with respect to the CH_2 protons; this is to be expected as the larger Fe–μ-O–Fe angle would engender structural variations which alter the conformations of the chelate rings and, therefore, the orientations of the methylene C–H bonds relative to the metal orbitals responsible for delocalizing unpaired spin density.[32] The NMR spectra of **1–3** are essentially the same, suggesting that their structures in solution are identical.

EPR Studies. EPR spectra were recorded both in the powder form and in acetonitrile solution for complexes **1–4**. The EPR spectra for **2** in acetonitrile, shown in Figure 3A for orientations of the microwave magnetic field, B_1, parallel and perpendicular to the static field B, show an extremum at an applied field of 43 mT ($g \approx 15$). The intensity of this resonance for **2** is proportional

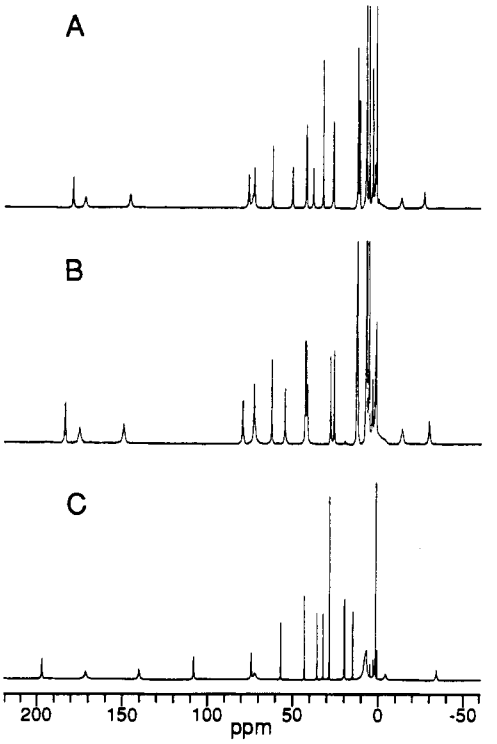

Figure 2. ^1H NMR spectra of diferrous complexes at 300 K: (A) $[Fe_2BPMP(O_2CC_2H_5)_2]BPh_4$ (**5**) in CD_2Cl_2; (B) $[Fe_2BPCP(O_2CC_2H_5)_2]BPh_4$ (**4**) in CD_2Cl_2; (C) $[Fe_2BPMP\{O_2P(OC_6H_5)_2\}_2]Cl$ (**1**) in CD_3CN. The broad signal at ~8 ppm in (C) is due to the ring protons on the bridging diphenyl phosphate.

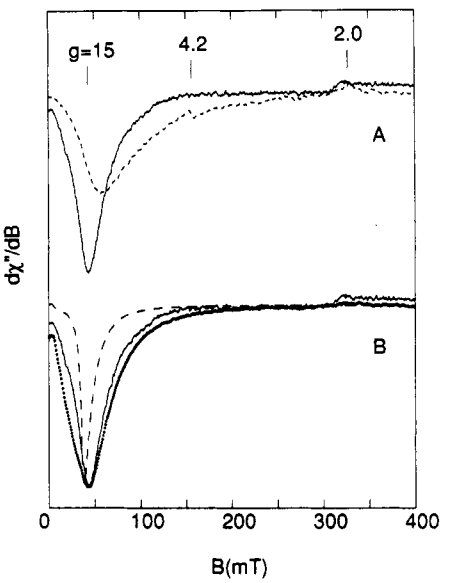

Figure 3. X-band EPR spectra at 20 K: (A) spectra of **2** 8.0 mM in CH_3CN/toluene with $B_1 \parallel B$ (—) and $B_1 \perp B$ (- - -); (B) spectra with $B_1 \parallel B$ of **2** in powder form (···) and **5** in acetonitrile (- - -, $T = 3$ K). The solid line in (B) is a copy of the solution spectrum with $B_1 \parallel B$ shown in (A). Instrumental parameters: microwaves, 0.2 mW at 9.2 GHz; modulation, 1mTpp at 100 kHz; gain, 2.5×10^4; dB/dt, 1.7 mT/s.

to the concentration of the sample, whereas the resonances at $g = 4.2$ and 2.0 have very weak and variable intensity and thus are assigned to impurities. The increase in intensity of the $g \approx 15$ resonance for $B_1 \parallel B$ indicates the associated metal center has integer electronic spin.[34] The resonance condition for such signals is $(h\nu)^2 = \Delta^2 + (g\beta B)^2$, where Δ is the zero-field splitting of the spin doublet which gives rise to the resonance. The powder spectrum of **2** (Figure 3B) is identical to the powder spectra of

(32) Bertini, I.; Luchinat, C. *NMR of Paramagnetic Molecules in Biological Systems*; Benjamin Cummings: Menlo Park, CA, 1986.

(33) Ming, L. J.; Jang, H. G.; Que, L., Jr. *Inorg. Chem.* **1992**, *31*, 359–364.

(34) Hendrich, M. P.; Debrunner, P. G. *Biophys. J.* **1989**, *56*, 489–506.

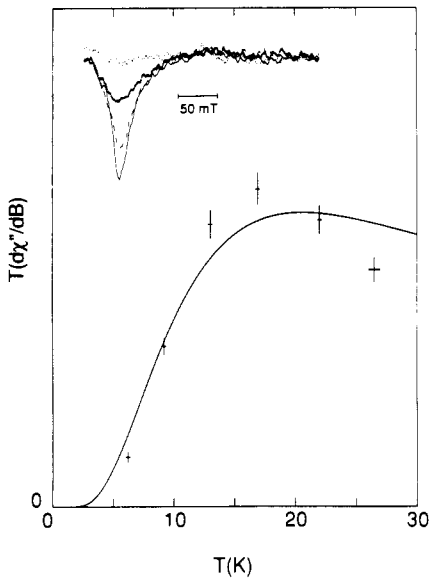

Figure 4. Temperature dependence of the $g = 15$ signal of Figure 3A. The signal intensity was determined from the depth of the trough at $B \approx 40$ mT; each data point together with its error is indicated by a cross. The theoretical line was calculated by diagonalization of equation 1 for $J = 1.5\ cm^{-1}$, $|D_i| = 10\ cm^{-1}$, and $E_i/D_i = 0$. The inset shows the normalized EPR spectra at the approximate temperatures 3 K (- - -), 10 K (—), 20 K (– –), and 30 K (···).

1 and **3** and similar to its spectrum in solution, indicating that the EPR properties of the complex cation are unperturbed by intermolecular interactions. The temperature dependence of the $g \approx 15$ resonance for **2** was carefully measured under nonsaturating microwave power with a thermometer frozen into the sample. The signal intensity times temperature is plotted versus temperature in Figure 4. As shown in the inset, the signal intensity has a maximum near 15 K and vanishes near 3 K, indicating that the signal originates from an excited state spin doublet. No change in the lineshape was observed over the temperature range studied. The observed temperature dependence corresponds to a system where this EPR active doublet is 12 cm^{-1} above the EPR silent doublet, i.e. the complex is antiferromagnetically coupled.

In contrast, **4** exhibits an intense X-band EPR signal with an extremum at an applied field of 40 mT ($g \approx 17$). This spectrum is identical to that observed for **5** (Figure 3B, dashed line). The signal intensity is greatest at 3 K and decreases with increasing temperature similar to **5**, indicating that the signal arises from the ground spin doublet. Thus, as in **5**, the iron sites of **4** are ferromagnetically coupled.

Several diferrous proteins and model complexes exhibit EPR signals similar to those shown in Figure 3.[9-11,16] The interpretation of these spectra can be simplified by dividing the problem into regimes characterized by the ratio of the exchange to zero-field energies.[10] This approach facilitates prediction of the properties of the spectroscopically important low lying levels.

For weak ferro- or antiferromagnetic coupling ($|J/D_i| < 1/3$), the lowest pair of levels of each $S = 2$ ferrous site couple to form the quartet shown in the center of Figure 5 for $D_i < 0$. Only one of the doublets of the quartet is predicted to be EPR active with $g \approx 16$. The EPR active doublet is the ground doublet for $J < 0$ (ferromagnetic) and the excited doublet for $J > 0$ (antiferromagnetic coupling).[10] In a recent study, the integer-spin EPR spectrum observed for deoxyhemerythrin azide was identified to originate from the ground doublet of this quartet.[10] This assignment was based on an electronic model that gave matching spectral simulations, the correct temperature dependence of the signal, and an accurate spin quantitation of the sample. Moreover, this model was found to be in good agreement with an independent analysis of the magnetization data. These results and similar

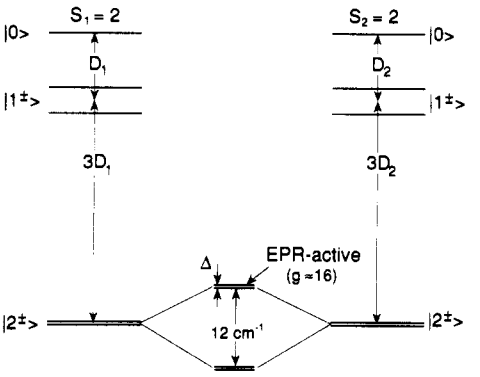

Figure 5. Energy levels in the weak coupling scheme for $D_i < 0$, $E_i/D_i \approx 0$, and $J > 0$ (antiferromagnetic coupling). The EPR active doublet is split in zero field by Δ. Application of a magnetic field will split that spin doublet in energy by $(\Delta^2 + (g\beta B)^2)^{1/2}$.

agreements with Mössbauer spectroscopy for other complexes[35] indicate that the method of analysis for EPR spectra is well founded.

For strong ferromagnetic coupling ($J/D_i > 1$), the ground multiplet of the diferrous pair is closely identified as $S = 4$.[36] The EPR spectra of complexes **1–3**, however, are incompatible with an assignment to a doublet from within this S = 4 multiplet. This is evident upon comparison with the spectra published previously for the related complex **5**,[16] shown in Figure 3B. The EPR signal for **5** occurs at significantly lower field (both the position of the valley and the high field edge) than those of complexes **1–3**, and it is already at the high field limit (within 3 mT) of all possible calculated spectra for the relevant doublets of an $S = 4$ multiplet. The spectra of complexes **1–3** have signal intensity at significantly higher field than is predicted through spectral simulation of an $S = 4$ multiplet.

The high field position of the $g \approx 15$ signal also cannot be simulated in the weak coupling regime under conditions applicable to our earlier studies. Again, the experimental spectra have significant intensity at magnetic fields higher than can be predicted by simulation. The lack of a fit suggests that one of three simplifying assumptions imposed on the weak coupling model is not valid. These assumptions, which are not relevant for the strong coupling model, are (a) that the perturbation expressions of equation 5 in reference 10 are sufficiently good approximations, (b) that the magnitudes of the zero-field energies of each iron site are equivalent ($D_1 = D_2$), and (c) that the electronic coordinate systems for the iron sites are equivalent ($\mathbf{D}_1$ tensor is not rotated relative to $\mathbf{D}_2$ tensor).

To address the problem, a new computer program was constructed which calculates EPR spectra via diagonalization of the full 25 × 25 matrix representation of equation 1. The resulting simulations from this program gave the same inadequate fits for magnitudes of D_1 unequal to D_2, indicating that the lifting of assumptions a and b alone is insufficient. The resolution of the problem appears to require a rotation of the electronic coordinate system of one iron site relative to the other, i.e. assumption c is invalid. While it is not yet possible to provide accurate simulations, and therefore no spin quantitation, an angle of 60° between the easy axes of magnetization[37] of the iron sites results in a shift in the calculated spectrum sufficient to match the high field edge of the experimental spectra of complexes **1–3**, *a result thus far not achieved by any other means*. Thus the high field position of the $g = 15$ signal is compatible with the weak coupling model,

(35) Juarez-Garcia, C.; Hendrich, M. P.; Holman, T. R.; Que, L., Jr.; Münck, E. *J. Am. Chem. Soc.* **1991**, *113*, 518–525.
(36) See Figure 3 of reference 11b for a digram of the $S = 4$ multiplet. For strong antiferromagnetic coupling, the ground state is diamagnetic ($S = 0$) and does not give an EPR signal.

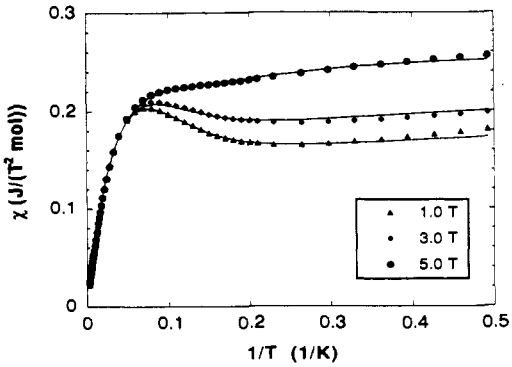

Figure 6. Magnetization of $[Fe_2BPMP\{O_2P(OC_6H_5)_2\}_2]BF_4$ (**2**) at three fields over the temperature range 2–300 K. Data are plotted as molar susceptibility (χ_{mol}) versus inverse temperature. A least-squares fit to the data found $J = 2.0$ cm^{-1}, $|D_i| = 14$ cm^{-1}, $E_i/D_i = 0.23$, and $g_i = 2.11$ (solid lines). The calculation assumes identical ferrous sites with coaxial zero-field splitting tensors and diagonalizes the full 25 × 25 spin Hamiltonian of equation 1.

provided that the zero field splitting tensors of the individual ferrous centers of the diferrous complex are rotated relative to each other.

The temperature dependence of the $g = 15$ signal (Figure 4) indicates that it originates from an excited doublet 12 cm^{-1} above the EPR silent ground doublet, thus implicating a system with weak antiferromagnetic coupling. Under the assumption of equal and coaxial D_i-tensors, the excited doublet is calculated to be at an energy of $8J$ above the ground state; thus the temperature dependence of the resonance corresponds to $J = 1.5$ cm^{-1}. However the energy splitting between the EPR active and inactive doublets depends on the angle between the easy axes of magnetization (see Figure 7 in reference 10), so the value of J determined from the temperature dependence of the EPR signal will be affected. For a rotation of 60°, the splitting between the EPR active and the EPR silent doublets is approximately $4J$, so the observed splitting of 12 cm^{-1} corresponds to an exchange energy of 3 cm^{-1}. Independent of the rotation, it is clear that the ground doublet is EPR silent, that the integer-spin signal originates from the first excited doublet at an energy of 12 cm^{-1}, and that the exchange coupling is weakly antiferromagnetic.

Magnetization Studies. Magnetization data of a polycrystalline sample of **2** show that the complex indeed exhibits weak antiferromagnetic coupling. Data collected at fields of 1.0, 3.0, and 5.0 T, over the temperature range 2–300 K are plotted as molar susceptibility (χ_{mol}) versus inverse temperature at the three fields (Figure 6). The maximum in the 1 T data at a temperature of 15 K is indicative of antiferromagnetic coupling. It is also characteristic of an antiferromagnetic system with weak coupling to exhibit the largest susceptibility values for the highest field applied in the low temperature range (2–15 K).[38] The solid lines are least-squares fits calculated by diagonalization of the 25 × 25 spin Hamiltonian of equation 1 under the assumption of equal and coaxial $\mathbf{D}_i$ tensors. The final parameter set of the best fit was $J = 2.0$ cm^{-1}, $|D_i| = 14$ cm^{-1}, $E_i/D_i = 0.23$, and $g_i = 2.11$. This value of J is close to that obtained from EPR measurements under the same model constraints.

The EPR data, however, suggest that the electronic coordinate system of one iron center is rotated relative to the other. Thus, further least-squares fitting was also performed for an angle of 60° between the easy axes of magnetization of the Fe^{II} sites. An equally good fit to the magnetization data was achieved for $J = 2.5$ cm^{-1}, $|D_i| = 11$ cm^{-1}, $E_i/D_i = 0.31$, and $g_i = 2.11$. Thus, the value of J is again in agreement with that determined from the EPR data with the new constraints. The fit with rotation is presented not as measurement of the rotation, but rather as evidence that the magnetization data do not rule out such a rotation. The confirmation of rotated electronic tensors will require a parameter set consistent with the collective data from high field Mössbauer, magnetization, and EPR measurements. Since the EPR signal transition probability can be significantly affected by a rotation of D_i-tensors in the weak coupling regime, the spin quantitation of the sample will also provide an important check of consistency; these experiments are in progress.

The demonstration in this paper that integer spin EPR analysis and saturation magnetization experiments independently afford a description of the electronic structure of $[Fe_2BPMP\{O_2P(OC_6H_5)_2\}_2]^+$, following the weak coupling scheme proposed by Hendrich et al., enhances the utility of the EPR method when applied to metalloproteins. Metalloproteins often have multiple magnetic species which render magnetization data for such systems difficult to interpret. Integer spin species in such proteins can however be analyzed on the basis of their EPR signals independent of the other magnetic species present.

Summary and Perspective

We have synthesized and characterized an antiferromagnetically coupled diferrous complex that exhibits an integer-spin EPR signal at $g \approx 15$, a resonance position similar to that found for the diferrous RNR R2 protein.[15] Our present efforts to simulate the signal from the synthetic complexes lay the groundwork upon which to base the analysis of the analogous signal observed for the R2 protein. It is clear that the strong coupling model is incompatible with the resonance position of the $g \approx 15$ signal. Furthermore some of the simplifying assumptions made in the original weak coupling model[10,16] do not apply to complexes **1**–**3** and the diferrous R2 protein. Our spectral simulations cannot reproduce the position of the $g \approx 15$ signal with the ferrous centers having coaxial $\mathbf{D}_i$ tensors; some rotation of the **D** tensors is required, which increases the number of parameters that need to be varied to fit the accumulated spectroscopic and physical data. At the present stage of our investigation, it is clear that such rotations can be accommodated with the available data. We plan a high field Mössbauer study of **1** to better define the boundaries of the parameter space used in our simulations.

The EPR signal of **1**–**3** has a temperature dependence that assigns it to an excited state that is 12 cm^{-1} above an EPR-silent ground state. Such properties can be easily accommodated by the weak coupling scheme first proposed for the diferrous centers of deoxyHrN_3 and MMO.[10,11b] While these protein signals derive from ground state doublets of putative ferromagnetically coupled diferrous centers, the fact that an excited state signal from an antiferromagnetically coupled diferrous complex can be rationalized by the same scheme further corroborates the validity of this proposed model and its generality. The possibility of observing this excited state signal stems from the weakness of the antiferromagnetic coupling that allows population of the excited state at a temperature low enough to prevent obliteration of the EPR signal by relaxation processes.

The excited state signal observed for **1** is in contrast to related ground state EPR signals found for **4** and **5**. It appears that replacing carboxylate bridges with phosphate bridges changes the metal–metal interactions from ferromagnetic to antiferromagnetic. We attribute this change to the large bite of the phosphate group, which affords a much larger Fe–O–Fe angle in **1**. The M–μ-O–M angle is an important factor in modulating the metal-metal interaction in dinuclear copper(II) complexes,

(37) The easy axis of magnetization is the axis with the largest spin expectation $\langle S_i \rangle$ in the presence of a magnetic field. In other words, for a system with high magnetic anisotropy (e.g. Fe^{II}), it is the axis along which the molecule is most easily made magnetic. Given sufficiently large magnetic field and anisotropy, a single crystal of the molecule would actually rotate to align this axis with the magnetic field. For $D < 0$ (> 0), this is the z (y) axis of the electronic **D** tensor.

(38) Yu, S.-B.; Wang, C.-P.; Day, E. P.; Holm, R. H. *Inorg. Chem.* **1991**, *30*, 4067–4074.

with larger angles favoring stronger antiferromagnetic interactions.[39] A similar systematic study is not available for diferrous complexes, but the data summarized in Table III suggest that such a correlation may be applicable. Another factor to consider is the length of the Fe–μ-O bonds, which have been shown to modulate the size of J in (μ-oxo)diferric complexes.[40] As can be seen from a perusal of Table III, the complexes with μ-hydroxo (**6**) or alkoxo bridges (**7**) show J values that are about an order of magnitude larger than the μ-phenoxo complex **1**, despite respectively having smaller or comparable Fe–μ-O–Fe angles. At present, the relative importance of the two factors in determining the sign and magnitude of the metal–metal coupling interaction is not established, given the limited number of complexes available in the database; however, within the μ-phenoxo subset, it is clear that the Fe–μ-O–Fe angle plays an important role. Further studies along these lines should be carried out.

The synthetic diferrous complexes that afford integer-spin EPR signals thus far all have at least one single atom bridge which mediates the metal-metal interaction that gives rise to these signals. Deoxyhemerythrin (deoxyHr) azide fits this pattern on the basis of the crystal structure of deoxyHr;[8a] an aqua bridge is proposed for the diiron unit in this complex.[9a] However it is not clear whether single-atom bridges are present in the diferrous forms of methane monooxygenase and ribonucleotide reductase, both of which exhibit integer spin EPR signals.[11b,15] Indeed for both enzymes there are some indications that a single-atom bridge may not be present. EXAFS studies have failed to detect the presence of an Fe–Fe vector in reduced MMO.[4d] In a dinuclear center, the contribution of the Fe–Fe scattering to its EXAFS spectrum diminishes as the vibrational motions of the two ions become more independent of each other.[8c] Thus the absence of a single-atom bridge would be consistent with the EXAFS data; it is also possible that the single-atom bridge may be bound so weakly to the two ferrous ions that their vibrational motions would not be strongly correlated. The crystal structure of the dimanganese(II) derivative of the R2 protein of ribnucleotide reductase shows a dinuclear center that is bridged only by two carboxylates in an *O,O'* fashion;[41] the corresponding diiron(II) derivative may also adopt the same structure. It is not clear at present whether the observation of these low field integer spin EPR signals demands the presence of a single-atom bridge to mediate the metal-metal interaction. We are just beginning to understand the principles by which an $Fe^{II}_2(\mu\text{-OR})$ unit can give rise to such signals. It remains to be seen whether carboxylate bridges alone can mediate the required interactions; synthetic efforts are needed to alleviate the present paucity of complexes of this type.

Acknowledgment. We are grateful to Professor J. D. Britton for his expertise in the X-ray diffraction experiments. We thank to Dr. T. A. Kent and Prof. E. P. Day for providing the magnetization fitting program. This work has been supported by National Institutes of Health Grant GM-38767 (L.Q.).

Supplementary Material Available: Tables of the atomic coordinates, thermal parameters, bond lengths, and bond angles for $[Fe^{II}_2BPMP\{O_2P(OC_6H_5)_2\}_2]Cl\cdot 2CH_2Cl_2\cdot H_2O$ (**1**) (23 pages). Ordering information is given on any current masthead page.

(39) Willet, R. D. In *Magneto-Structural Correlations in Exchange Coupled Systems*; Willett, R. D., Gatteschi, D., Kahn, O., Eds.; D. Reidel Publishing Co.; Dordrecht, The Netherlands, 1985; pp 389–420 (see also references therein).

(40) Gorun, S. M.; Lippard, S. J. *Inorg. Chem.* **1991**, *30*, 1625–1630.

(41) Atta, M.; Nordlund, P.; Aberg, A.; Eklund, H.; Fontecave, M. *J. Biol. Chem.* **1992**, *267*, 20682–20688.